Flow analysis of the polymer spreading during extrusion additive manufacturing

Jean-François Agassant, Franck Pigeonneau, Lucas Sardo, Michel Vincent

Flow Analysis of the Polymer Spreading during Extrusion Additive Manufacturing

J.-F. Agassant, F. Pigeonneau, L. Sardo, M. Vincent

MINES ParisTech, PSL Research University, CEMEF - Centre for material forming, CNRS UMR 7635, CS 10207, rue Claude Daunesse 06904 Sophia Antipolis Cedex, France

Abstract

The spreading of molten polymer between the moving printing head and the substrate in extrusion additive manufacturing is studied. Finite element computation and an analytical model have been used. The hypotheses of the analytical model are qualitatively justified by the results of the numerical computation. The analytical calculation is a powerful tool to rapidly evaluate the relationships between processing parameters (extrusion rate, printing head velocity, gap between the printing head and the substrate) and some characteristics of the deposition (dimensions of the deposited filament, pressure at the printing head nozzle, separating force between substrate and printing head). An isothermal hypothesis is discussed. The viscous non-Newtonian behavior is accounted for through an approximate shear thinning power law model. A printing processing window is defined following several requirements: a continuous deposit, without spreading in front of the printing head, maximum and minimum spreading pressures, an upper-limit for the separating force between head and substrate.

Key words: Polymer; Extrusion; Additive manufacturing; Deposition; Modeling

1. Introduction

Additive manufacturing technologies were first developed in the 1980s, mainly for rapid prototyping. With their growing efficiency they are now applied to the production of parts with mechanical requirements. One of the most widely used polymer additive manufacturing technology is extrusion deposition, sometime called fused filament fabrication (FFF). A solid filament of material is fed into a vertical printing head via a pinch roller mechanism. The polymer is melted in the heated bottom part of the printing head. Finally, the molten polymer flows through a nozzle which moves generally in a horizontal plane to lay down a layer of molten polymer on a surface formed by the preceding deposited layers.

Concerning the flow and the heat transfer, the literature on extrusion additive manufacturing is focused on the fusion phenomena in the printing head [1, 2, 3, 4] and on the thermal phenomena within the successive deposited layers (fusion and re-melting). This governs the welding and the filling of porosities [5, 6, 7] and so, the mechanical properties of the part.

Very few papers are devoted to the deposition itself. Crokett [8] considered that the distance between the bottom of the printing head and the substrate is important. This means that there is a free surface analogous to what is observed in the curtain coating process. As a consequence, the leading parameter to be accounted for is the surface tension [8, 9].

*Corresponding author: Tel. +33 (4) 93 95 74 12, Fax +33 (4) 92 38 97 52.

Email address: michel.vincent@mines-paristech.fr (M. Vincent)

Very few papers consider the shearing and pressure phenomena occurring when the distance between the printing head is lower than the internal nozzle diameter. This represents the more general printing situation [5]. The pressure will obviously greatly influence the filling of porosities and the welding with the previously deposited polymer. Recently, Du et al. [10] and Comminal et al. [11] have calculated the shape of the deposited layer and the pressure distribution between the moving printing head and the substrate using finite volume methods. Du et al. [10] accounted for a Non-Newtonian temperature dependent behavior of the polymer, but the widening of the deposit during spreading remained limited. Comminal et al. [11] used a Newtonian isotherm hypothesis and provided pressure distributions and deposit dimensions for different gaps between the head and the substrate and different fluid and printing head velocities. Xia et al. [12] computed the deposit of successive layers. They used viscous and elastic behaviors in the liquid and solid phases respectively, but they did not calculate the pressure generation between the printing head and the substrate.

The objective of this paper is to analytically calculate the spreading of the molten polymer between the moving printing head and the substrate. This allows to quickly show the influence of the processing parameters (extrusion velocity, printing head velocity, gap between the printing head and the substrate) and of the rheology of the molten polymer on the dimensions of the deposited layer (thickness and width), on the pressure exerted on the printing head and on the resulting separating force between the head and the substrate. This model also allows defining operating conditions (i) without polymer build up in front of the printing head that occurs when the nozzle velocity is too small compared to the extrusionone as well as (ii) avoiding discontinuous polymer deposition which can occur when the nozzle velocity is too high in comparison to the extrusion velocity. The analytical calculation requires simplifications of the flow kinematics. A 3D finite element numerical computation without any kinematics assumption has been developed to evaluate the validity of the assumptions required for the analytical approach.

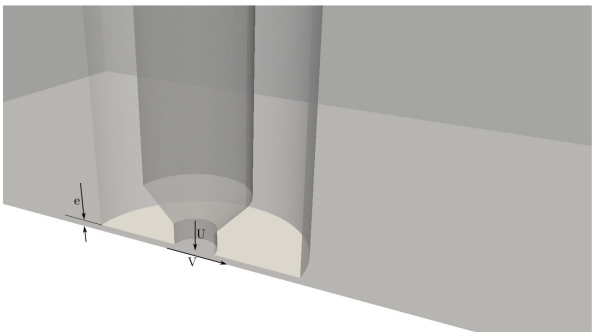

Figure 1: Perspective view of the 3D printing head and surrounding domain. Only half of the domain is considered.

2. Model description

2.1. Justification of an analytical approach: 3D Finite elements spreading model

A Newtonian isothermal finite element computation of the fluid spreading on a substrate has been performed using the CIMLIB-CFD Library [13, 14]. The shape of the deposited layer, the free surface between the printing head and the substrate, the pressure field have all been computed for different processing parameters: the average fluid velocity at the nozzle exit U, the printing head velocity V and the gap between the nozzle and the substrate e. Fluid interfaces are tracked implicitly with a level-set method [15]. The geometry of the domain, depicted in Figure 1, includes the printing head, the substrate and the surrounding air. The external surface of the head is cylindrical. Its internal surface is also a cylinder which diameter is close to the feeding filament one, followed by a convergent and a final smaller cylindrical region at the exit. Due to the symmetry of the problem, only one half of the domain is considered. The Galilean referential is attached to the 3D printing head so that the substrate moves with a constant velocity V.

Both fluids are considered incompressible media so that mass conservation reduces to Eq. (1). The dynamic viscosity of the polymer and surrounding air are respectively η_1 and η_2. In the momentum conservation Eq. (2) inertia and gravity forces as well as surface tension are neglected. Surface tension is

important after spreading of the polymer on the substrate, but has no influence for the flow analysis between the printing head and the substrate.

$$\boldsymbol{\nabla} \cdot \boldsymbol{u} = 0, \tag{1}$$

$$-\boldsymbol{\nabla} p + \boldsymbol{\nabla} \cdot [2\eta(\varphi)\boldsymbol{D}] = 0, \tag{2}$$

$$\frac{D\varphi}{Dt} = 0. \tag{3}$$

The prime unknowns are the velocity $\boldsymbol{u}$, pressure p and level-set function φ which allows tracking the polymer–air interface. The evolution of φ is obtained by solving Eq. (3). The level-set function φ is used to determine the dynamic viscosity at any point in the fluid domain. $\boldsymbol{D}$ is the rate-of-strain tensor. A sticking contact is assumed between the polymer and both the bottom of the printing head and the substrate. The governing equations are numerically solved using a finite element formulation according to the recent developments presented in [13] wherein details about the discretization and adaptive meshing can be found. The computation starts with an initial volume of polymer outside the nozzle and progresses as a function of time till a stabilized deposited layer is obtained.

The internal and external nozzle radius are respectively $R_i = 0.2$ mm and $R_e = 1$ mm. The gap between the nozzle and the substrate is $e = 0.12$ mm. Polymer and air viscosities are respectively $\eta_1 = 10^3$ Pa·s and $\eta_2 = 1.7 \cdot 10^{-5}$ Pa·s. The polymer viscosity corresponds to the viscosity of the ABS used by Mackay et al. [3] at 230°C and at an average shear rate between the moving head and the substrate. Coogan and Kazmer [16] recently studied the rheology of polystyrene and polycarbonate filaments used in additive manufacturing. They point out lower values of viscosity, between 200 and 400 Pa·s for different temperatures and the same average shear rate. The computed pressure values which will be shown later on Figs. 5 and 9 are purely proportional to the viscosity value, so it is possible to infer from these results the pressure for any polymer.

The relevant non-dimensional parameter is the ratio of the velocity at the nozzle to the printing head velocity, U/V. Two numerical runs have been done with U/V equal to 1 and 1/2.

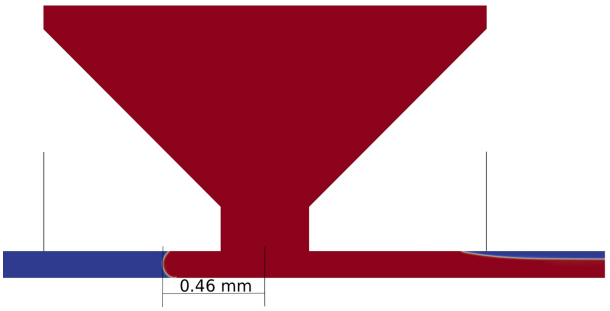

Figure 2: Side view of the polymer spreading in steady-state regime for a ratio $U/V = 1$.

Figure 2 and Figure 3 respectively depict the side and top views of the polymer spreading for $U/V = 1$ with $U = V = 32$ mm/s. This corresponds to an extrusion flow rate $Q = 4$ mm^3/s. The polymer spreads in front of the nozzle on a distance from the nozzle axis equal to 0.46 mm. In the lateral direction, the fluid reaches a maximal half-width equal to 0.80 mm, which is 1.63 times the distance in front of the nozzle. The thickness of the deposited layer (h) is approximately constant and less than the gap (0.079 mm corresponding to 70% of the gap e). Its half-width is 0.73 mm (Figure 4).

Figure 2 and Figure 3 respectively depict the side and top views of the polymer spreading for $U/V = 1$ ($U = V = 32$ mm/s). The polymer spreads in front of the nozzle on a distance from the nozzle axis equal to 0.46 mm. In the lateral direction, the fluid reaches a maximal half-width equal to 0.80 mm, which is 1.63 times the distance in front of the nozzle. The thickness of the deposited thread (h) is approximately constant and less than the gap (0.079 mm corresponding to 70% of the gap e). Its half-width is 0.73 mm (Figure 4).

Figure 5 shows the pressure distribution between the moving head and the substrate. A maximum pressure of 7 MPa is obtained just at the nozzle exit. This pressure, proportional to the chosen Newtonian viscosity, would be much smaller with a shear-thinning behavior.

Figure 6 and Figure 7 show the side and top views

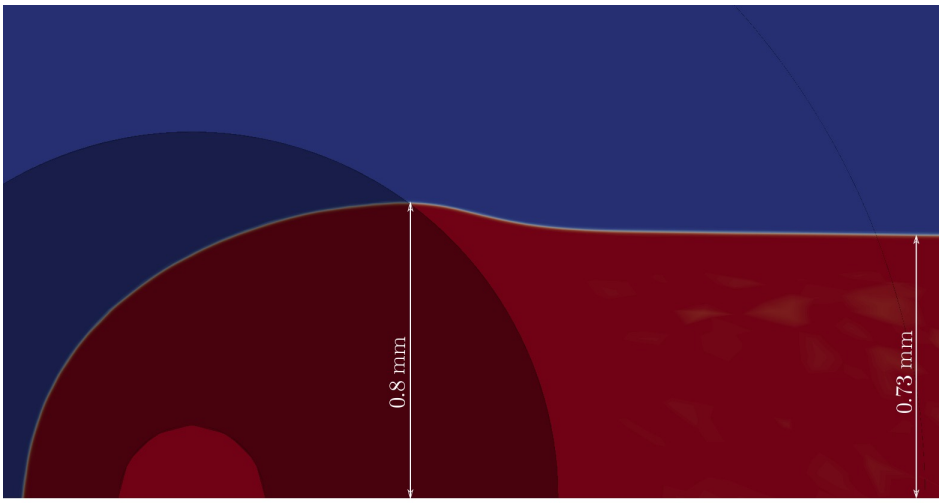

Figure 3: Top view of the polymer spreading in steady-state regime for a ratio $U/V = 1$ taken at a distance from the substrate equal to $e/2$.

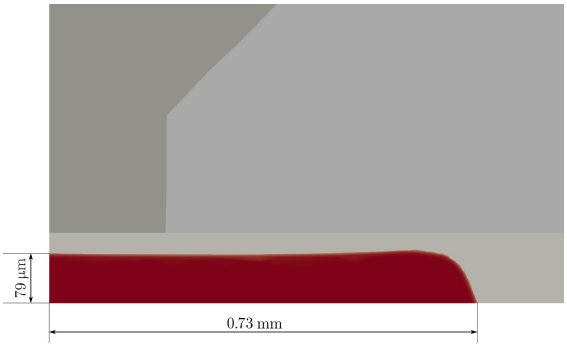

Figure 4: Front view of the polymer filament at a distance equal to 3 mm downward to the printer head in the case of $U/V = 1$.

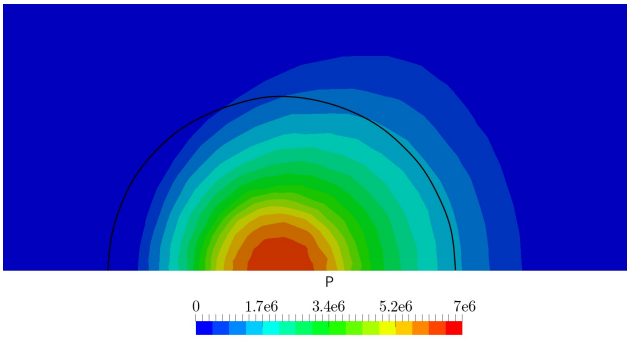

Figure 5: Pressure field (in Pa) under the printer head taken at a distance from the substrate equal to $e/2$ when $U/V = 1$.

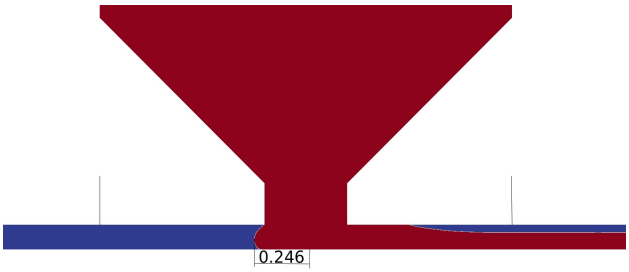

Figure 6: Side view of the polymer spreading in steady-state regime for a ratio $U/V = 1/2$.

of the polymer spreading for $U/V = 0.5$ ($U = 16$ mm/s and $V = 32$ mm/s). This corresponds to an extrusion flow rate $Q = 2\,\mathrm{mm}^3/\mathrm{s}$. Since the extrusion velocity is less than the head velocity, the polymer flows in an upward direction over a smaller distance equal to 0.246 mm (0.046 mm upwards the internal nozzle edge). The polymer leaves the contact with the bottom of the printing head before the periphery (the external diameter) of the printing head. The maximum pressure at the nozzle exit shown on Figure 9 is 1.8 MPa. It is much less important than in the previous case (7 MPa). A pressure decrease by a factor 2 could be expected when decreasing the flow rate by a factor 2, but the shape of the deposited layer is different and the surface of contact of the polymer with the bottom of the printing head is less important with the smaller flow rate, explaining the much larger pressure decrease. The polymer spreads laterally over a smaller distance than before as shown in Figure 7 and Figure 8. The minimum thickness of the deposited layer is equivalent to the previous case in agreement with the results of Comminal et al. [11] but its shape is less regular and its width is reduced by more than a factor 2.

These preliminary computations are in line with the previous results obtained by Comminal et al. [11] showing that the thickness of the deposited layer is less than the gap e. The computational fluid dynamics (CFD) is a powerful tool in which multiphysics can be taken into account, for example a non-uniform temperature field at nozzle exit and a shear thinning behavior for the molten polymer. However, and even if the computing power is still increasing, the screening of design and working conditions stay a hard task in CFD. For optimization purpose, it is useful to develop an approximate analytical method based on assumptions coming from these preliminary computations. Such a model allows for rapid testing of the sensitivity of pressure, separating force, dimensions of the deposited layer, to the geometry of the printing head and the processing parameters. It will also help defining the processing window for a continuous deposit without polymer deposit built up in front of the printing head.

2.2. Equations of the 2D mechanical model

As in Section 2.1, gravity, inertia and surface tension are neglected. A sticking contact of the polymer with the bottom of the printing head and with the substrate is considered. The numerical computation shows that this is valid for $U/V = 1$, but less valid for $U/V = 1/2$ where the contact between the polymer and the bottom of the printing head is left before the periphery of the head. The flow is assumed to be isothermal. This will be discussed in section 2.4. The polymer is assumed to be a Newtonian fluid, but an equivalent Newtonian viscosity η corresponding to the average shear rate between the printing head and the substrate, Eq. (4), will be considered to roughly take into account the shear thinning power-law behavior, Eq. (5), where K is the consistency and n is the power-law index:

$$\dot{\gamma} = \frac{V}{e}, \tag{4}$$

$$\eta = K\dot{\gamma}^{n-1}. \tag{5}$$

The kinematics of the layer deposit is sketched on Figure 10 in the (x, y) plane, where x is the printing head displacement direction and y is perpendicular to the substrate located in the plane (x, z) at $y = 0$, the z axis being perpendicular to the (x, y) plane. The velocity field is assumed to have only one non-zero component along the x direction, v_x. This means that the complex flow for $-R_i < x < R_i$ and

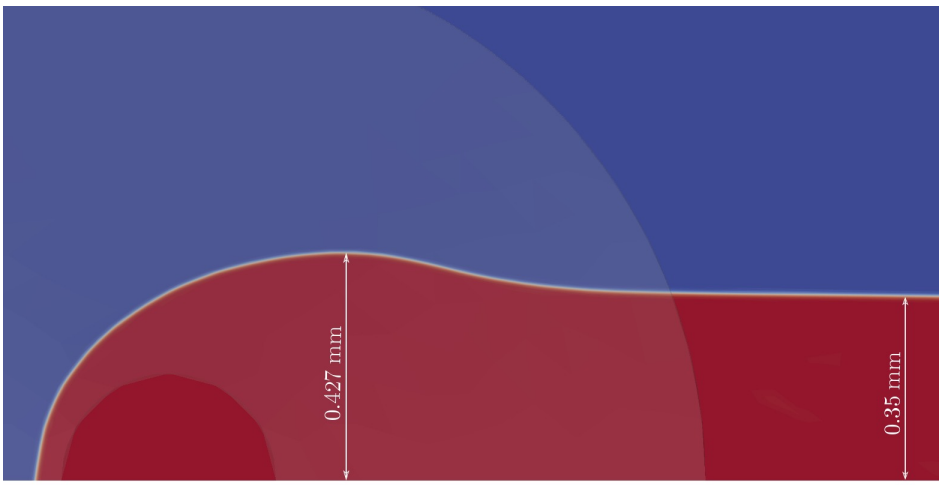

Figure 7: Top view of the polymer spreading in steady-state regime for a ratio $U/V = 1/2$ taken at a distance from the substrate equal to $e/2$.

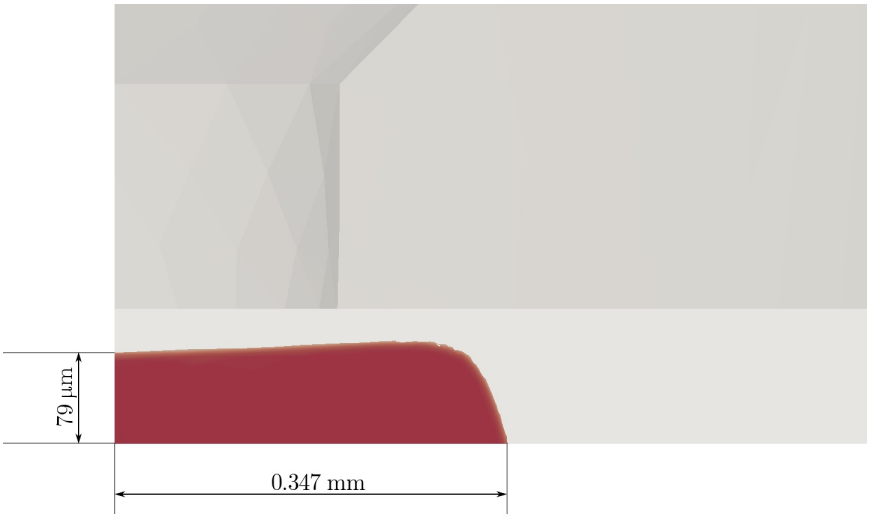

Figure 8: Front view of the polymer filament at a distance equal to 3mm downward to the printer head in the case of $U/V = 1/2$.

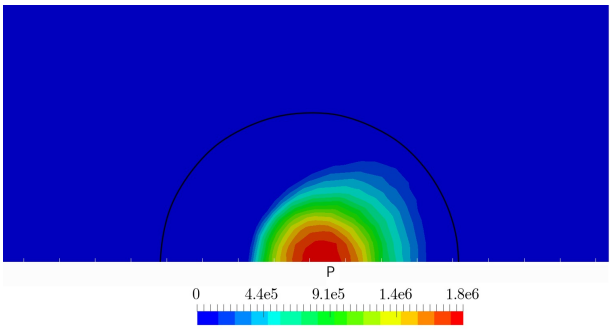

Figure 9: Pressure field (in Pa) under the printer head taken at a distance from the substrate equal to $e/2$ when $U/V = 1/2$.

$0 < y < e$ below the nozzle exit is neglected. This velocity profile is different in the downstream direction (negative value of x) and in the upstream direction (positive x).

The molten polymer flow rate Q in the nozzle and therefore the average velocity U is related to the imposed solid filament velocity.

As in the previous numerical model, the printing head is fixed and the substrate (assumed to be planar) is moving at a constant distance e below the printing head and at a constant velocity V in the negative ($x-$) direction. Therefore, the polymer is sheared between the nozzle and the moving substrate. At the nozzle outlet the pressure is P_0. It decreases to atmospheric pressure at the printing head periphery for $x = -R_e$. In the same way it will also decrease to atmospheric pressure level in the forward direction at $x = L$, which is an unknown of the problem. The superposition of these shear and pressure flows will be responsible for the development of a pressure field and a separating force exerted on the printing head. These are important parameters of the printing process.

The solution of the Stokes equations in the deposit direction (for $x < 0$) gives the deposit rate per unit width q. It is the sum of a simple shear flow induced by the velocity V and a pressure flow induced by P_0 on a distance (R_e–R_i), Eq. (6). This equation relies on the fact that the polymer remains in contact with the bottom of the printing head up to $x = -R_e$.

$$q = V\frac{e}{2} + \frac{1}{12\eta}\frac{P_0}{R_e - R_i}e^3. \tag{6}$$

In the forward direction ($x > 0$), the flow rate per unit width is nil and is the sum of the same shear flow and of a negative pressure flow induced by P_0 on a length L:

$$0 = V\frac{e}{2} - \frac{1}{12\eta}\frac{P_0}{L}e^3. \tag{7}$$

This leads to the value of L:

$$L = \frac{P_0 e^2}{6\eta V}. \tag{8}$$

2.3. From the 2D analytical mechanical model to a 3D approximate model

This 2D model is unable to predict the width of the deposited layer. We assume that the polymer spreading in the direction z perpendicular to the (x, y) plane is of the same order of magnitude as the spreading in front of the nozzle (Figure 11). This is not far from the numerical results when U/V is small (Figure 7). It remains qualitatively correct when U/V is more important (Figure 3).

$$W = 2\left(R_i + L\right). \tag{9}$$

We also assume that the flow rate is uniform through the width which means that the thickness of the deposited layer is uniform too. This is consistent with Figure 4 and Figure 8. This writes in the deposit ($x < 0$) direction:

$$q = \frac{Q}{2\left(R_i + L\right)} = V\frac{e}{2} + \frac{P_0}{12\eta\left(R_e - R_i\right)}e^3. \tag{10}$$

Eqs. (7) and (8) are still valid. Replacing in Eq. (10) P_0 by its value derived from Eq. (8) leads to an equation of second order in L which has only one positive root:

$$L = \frac{-R_e + \sqrt{\left(R_e - 2R_i\right)^2 + 4\frac{Q}{eV}\left(R_e - R_i\right)}}{2}. \tag{11}$$

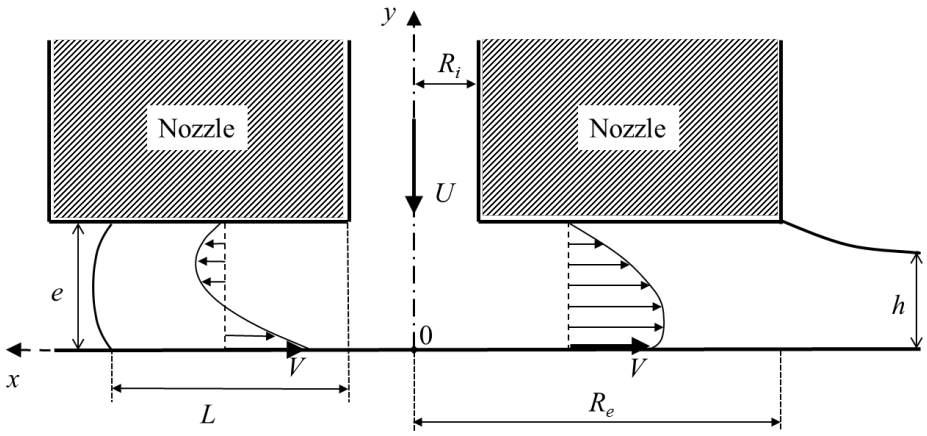

Figure 10: Analytical calculation domain.

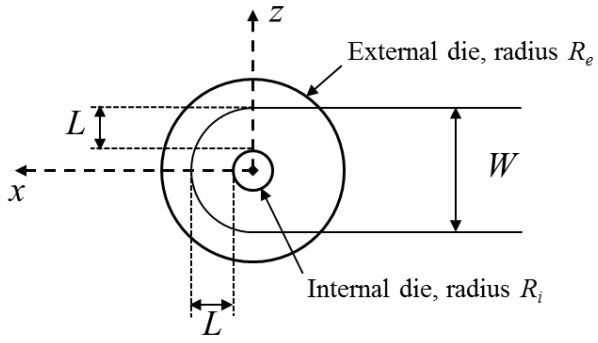

Figure 11: Approximate representation of the deposit shape in the substrate plane.

L depends on the nozzle dimensions R_i and R_e , the polymer flow rate Q, the gap between the printing head and the substrate e and the printing head velocity V. It does not depend on the polymer viscosity. The value of L, Eq. (11), leads to the width of the deposited layer W, and Eq. (10) to its thickness h:

$$h = \frac{Q}{WV} = \frac{e}{2} + \frac{P_0 e^3}{12\eta\left(R_e - R_i\right)V}. \tag{12}$$

In order to obtain a continuous deposit, P_0 needs to be positive and this leads to a first relationship:

$$h \geq \frac{e}{2}. \tag{13}$$

To avoid the molten polymer spreading in front of the printing head and so building a bad quality deposit, L needs to be less than $(R_e - R_i)$ which leads, from Eq. (8), to a second printing condition:

$$P_0 \leq \frac{6\eta V\left(R_e - R_i\right)}{e^2}. \tag{14}$$

Equations (12) and (14) imply $h \leq e$. The two limits for h are:

$$\frac{e}{2} \leq h \leq e. \tag{15}$$

The deposited thickness is between half the gap and the gap between the printing head and the substrate.

As $0 \leq L \leq R_e - R_i$, Eq. (9) leads to $2R_i \leq W \leq 2R_e$. Using Eq. (15) with $h = Q/(WV)$, one obtains:

$$\frac{Q}{2eR_e} \leq V \leq \frac{Q}{eR_i}. \tag{16}$$

These limit printing processing conditions do not depend on the polymer viscosity.

From the value of P_0 it is possible to have an estimate of the force exerted by the substrate on the printing head by multiplying P_0 by half of the surface of contact between the polymer and the printing head. Obviously the 3D computation of section 2.1 provides a more precise separating force value.

2.4. Comparison between the numerical and analytical models

To have a relevant comparison between computational and analytical models, we restrict the analytical calculation to the purely Newtonian case (without accounting for the shear thinning behavior, Eqs. (4–5).

The analytical dimensions of the deposited layer depend only on the printing head geometry, on the gap e between the printing head and the substrate (0.12 mm) and on the U/V ratio. Following Eq. (11), L writes:

$$L = \frac{-R_e + \sqrt{\left(R_e - 2R_i\right)^2 + 4\pi \frac{UR_i^2}{eV}\left(R_e - R_i\right)}}{2}. \tag{17}$$

- For $U/V = 1$, $L = 0.46$ mm. Following Eq. (9), $W_A = 1.32$ mm and $h_A = \frac{\pi R_0^2 U}{WV} = 0.095$ mm. The numerical results were: $W_N = 1.46$ mm and $h_N \simeq 0.08$ mm (average value in the width). The analytical maximum pressure at the nozzle is $P_{0,A} = 6.16$ MPa whereas the computed pressure is $P_{0,N} = 7$ MPa.

- For $U/V = 0.5$, $L = 0.21$ mm, $W_A = 0.82$ mm and $h_A = 0.076$ mm. The numerical results were: $W_N = 0.70$ mm and $h_N = 0.08$ mm. The analytical maximum pressure is $P_{0,A} = 2.88$ MPa as the computed pressure is $P_{0,N} = 1.8$ MPa.

Numerical and analytical results are of the same order of magnitude. Concerning the dimensions of the deposited layer there are less than 10 % difference for $U/V = 1$ and less than 16 % for $U/V = 0.5$. Nevertheless it can be observed that the computed deposited thickness is the same for both velocity ratios conditions whereas the analytical deposited thickness is significantly different. The numerical pressure overestimates the analytical pressure for $U/V = 1$, but underestimates it for $U/V = 0.5$. The analytical calculation assumes a sticking contact with the printing head whereas the numerical computation shows that the polymer leaves the contact before its periphery.

2.5. Preliminary approach of the thermal phenomena

The additive manufacturing of ABS is considered. The material parameters are taken from [3] and shown on Table 1. With these rheological data an equivalent Newtonian viscosity of 10^3 Pa·s which has been used in the numerical computation would correspond to a shear rate about 300 s^{-1}. It is in the range of the shear rates between the bottom of the printing head and the substrate.

The geometrical parameters are: $e = 0.1$ mm; $R_i = 0.2$ mm; $R_e = 1$ mm.

The flow rate induced by the filament velocity is $Q = 4$ mm^3/s. This corresponds to an average polymer velocity at the nozzle $U = 32$ mm/s. Following Eq. (16), a possible range for the printing head velocity is 20 mm/s $< V <$ 200 mm/s and so: $0.16 < U/V < 1.6$. The inlet temperature is $T_{\text{inlet}} = 220°\text{C}$.

2.5.1. Interfacial temperature

One assumes that there is no thermal resistance between the substrate (a previous polymer layer) and the new deposited layer. The interfacial temperature T_{int} is the average between the temperature of the substrate $T_{\text{substrate}}$ and the temperature of the new deposited layer. In our model it is equal to the nozzle temperature T_{inlet} which is supposed to be uniform and equal to the regulation temperature of the liquefier. This is obviously a strong hypothesis especially

Table 1: Material parameters of the ABS

Consistency K ($\mathrm{Pa{\cdot}s}^n$)	Power law index n –	Thermal conductivity k ($\mathrm{W{\cdot}m^{-1}{\cdot}K^{-1}}$)	Thermal diffusivity a ($\mathrm{m^2{\cdot}s^{-1}}$)	Glass transition temperature T_g (°C)
$1.26 \cdot 10^4$	0.55	0.21	$8.7 \cdot 10^{-8}$	100

at high extrusion flow rate.

$$T_{\text{int}} = \frac{T_{\text{inlet}} + T_{\text{substrate}}}{2}. \tag{18}$$

The temperature of the substrate depends on the time gap between the preceding deposited layer and the new one. It is related to the printing path followed by the printing head. Even if the substrate is at ambient temperature (20°C) the interfacial temperature is higher than the glass transition temperature ($T_{\text{int}} = 120$°C); in this extreme condition welding with the substrate is possible. Generally the substrate temperature is much higher, 100°C for example, which gives an interfacial temperature of 160°C.

2.5.2. Evaluation of the temperature profile

Assuming that the thin polymer layer between the substrate and the bottom of the printing head may be considered a semi-infinite body, the temperature field writes [17]:

$$\frac{T(y) - T_{\text{substrate}}}{T_{\text{inlet}} - T_{\text{substrate}}} = \text{erf}\left(\frac{y}{2\sqrt{at}}\right). \tag{19}$$

An estimate of the residence time between the nozzle exit and the periphery of the printing head is: $t = (R_e - R_i)/V$.

We compare on Figure 12 the temperature profile for the lowest ($V = 20$ mm/s) and the highest ($V = 200$ mm/s) printing head velocities at the periphery of the printing head for the two substrate temperatures previously mentioned, 20 and 100°C. At the lowest printing head velocity, the semi-infinite body condition is not respected and the temperature decrease in the deposited layer will be less important that what can be observed on Figure 12 because additional heat will be transferred from the printing head. At the highest printing head velocity, the semi-infinite body condition is valid. When increasing the molten polymer flow rate Q, the printing head velocity needs to increase too according to Eq. (16), and so the semi infinite body condition will be valid. The same result will be observed when increasing the gap e between the printing head and the substrate.

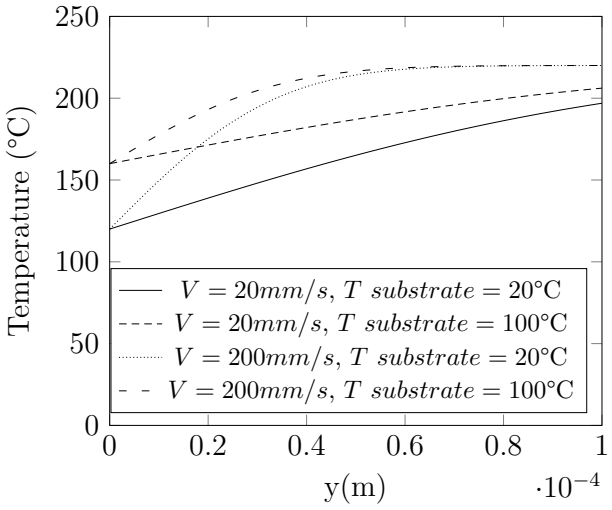

Figure 12: Temperature profile between the printing head and the substrate at the printing head outlet for two printing head velocities 20 and 200 mm/s and two interfacial temperatures 120°C and 160°C corresponding respectively to 20 and 100°C substrate temperatures.

2.5.3. Evaluation of the average temperature

The viscous dissipation may be important. The Brinkman number Br [17] represents the relative importance of the viscous dissipated energy and the energy lost by conduction with the substrate. For a power law behavior it writes:

$$\text{Br} = \frac{K\left(\frac{V}{e}\right)^{n-1} V^2}{4k\left(T_{\text{inlet}} - T_{\text{int}}\right)}. \tag{20}$$

The Brinkman number varies between 0.006 (for $T_{\text{int}} = 120$°C) and 0.009 (for $T_{\text{int}} = 160$°C) at the lowest printing head velocity ($V = 20$ mm/s) and between 0.20 and 0.33 for the highest printing head

velocity ($V = 200$ mm/s). When increasing the polymer flow rate Q, the printing head velocity needs to increase too and so does the Brinkman number. For example, $Q = 20$ mm^3/s results, according to Eq. (16), for the same gap e, to a printing head velocity: 100 mm/s$< V <$ 1000 mm/s. The highest possible printing head velocity is unrealistic and we limit this maximum velocity to 600 mm/s. In this extreme printing condition, the Brinkman number reaches high values (1.08 for an interfacial temperature of 120°C and 1.80 for an interfacial temperature of 160°C) and the viscous dissipation cannot be neglected.

When increasing the printing head velocity, the Brinkman number increases, but the residence time between the printing head and the substrate decreases. The Cameron number Ca (inverse of the Graetz number) [17] compares the residence time in the flow to the time for heat penetration. Assuming a shear dominant flow between the printing head and the substrate it writes:

$$\mathrm{Ca} = \frac{2a\left(R_e - R_i\right)}{Ve^2}. \tag{21}$$

Considering a fixed interface temperature with the substrate and an adiabatic heat transfer condition with the bottom of the printing head [17], the average temperature of the deposited layer at the printing head outlet (for $x = -R_e$) writes:

$$\overline{T} = T_{\mathrm{inlet}} + \frac{K\left(\frac{V}{e}\right)^{n-1} V^2}{3k}\left(1 - \frac{3}{4\mathrm{Br}}\right) \left[1 - \exp(-3\mathrm{Ca})\right]. \tag{22}$$

Figure 13 shows that this average temperature is significantly lower than the inlet temperature at low printing head velocity, especially for a substrate at ambient temperature. A slight temperature increase is observed for the highest printing head velocities.

As a conclusion, the isothermal hypothesis is valid, especially for a substrate temperature higher than 100°C and a printing head velocity higher than 100 mm/s. Its validity would obviously be improved when increasing the printing gap.

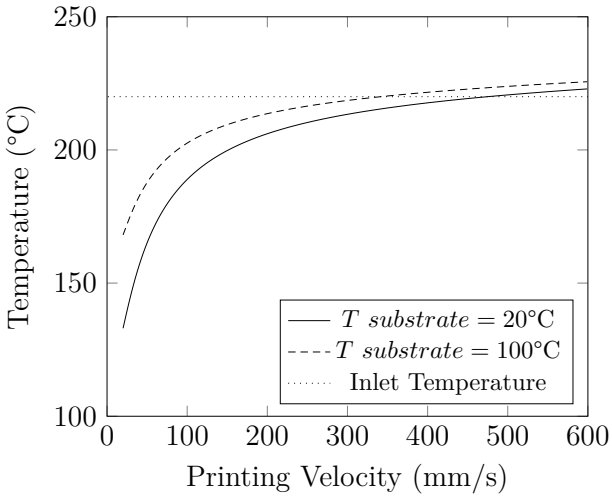

Figure 13: Gap-average temperature at the periphery of the printing head as a function of the printing head velocity for a substrate at ambient temperature and at 100°C.

3. Results

3.1. Influence of the printing head velocity V

As in paragraph 2.4, the gap is $e = 0.1$ mm, $R_i = 0.2$ mm, $R_e = 1$ mm. The polymer flow rate is $Q = 4$ mm^3/s, corresponding to an average extrusion velocity $U = 32$ mm/s. Figure 14 shows the dimensions of the deposited layer as a function of the printing head velocity. Its width varies between the nozzle diameter (0.4 mm) for the highest possible head velocity and the printing die diameter (2 mm) for the lowest possible one. Following Eq. (15) the deposited thickness varies between half of the prescribed gap (0.05 mm) and the gap (0.1 mm).

Figure 15 gives the pressure for the different head velocities. For V higher than 200 mm/s is nil and the deposit could be discontinuous. When V decreases the pressure increases. We assume two limits for P_0:

- Upper limit: the pressure on the solid feeding filament is the sum of and the pressure drop in the printing head, which has been computed for example in [1, 4]. If too important, it can induce filament buckling between the pinch roller mechanism and the top of the printing head [9]. We fix for example a maximum value of 5 MPa.

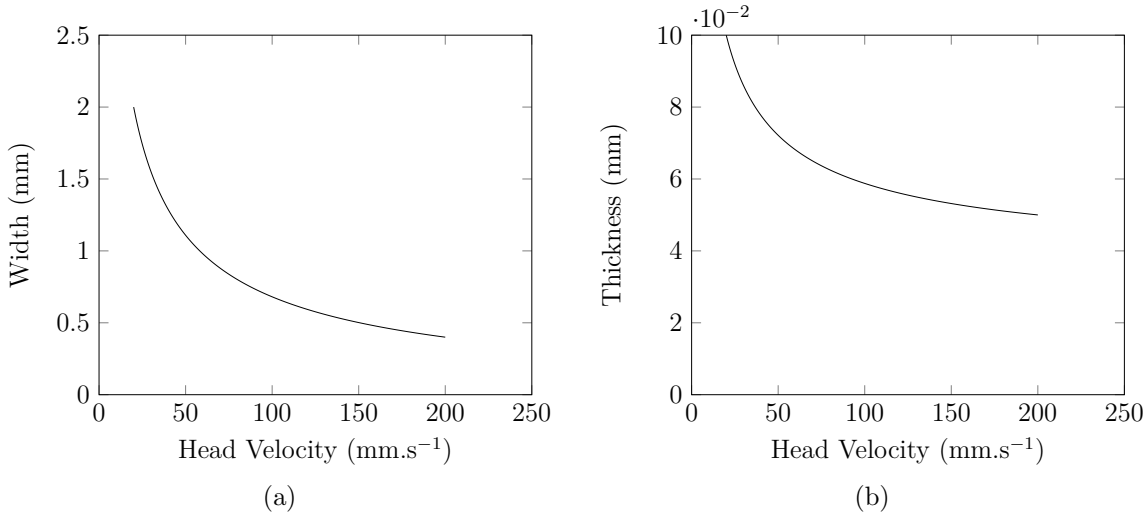

Figure 14: Width (a) and thickness (b) of the deposited layer as a function of the head velocity.

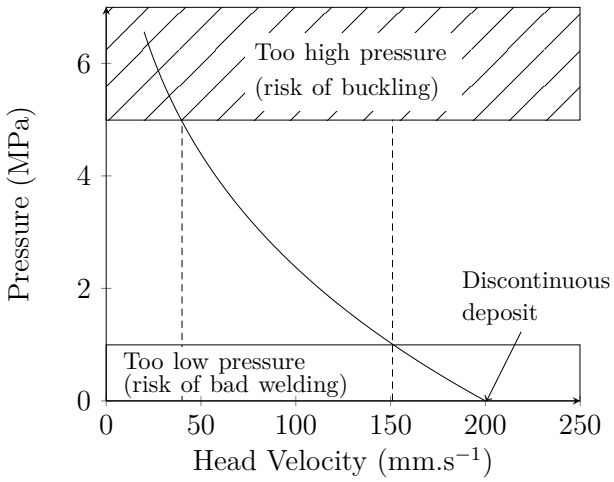

Figure 15: Pressure at the printing head nozzle outlet as a function of the printing head velocity.

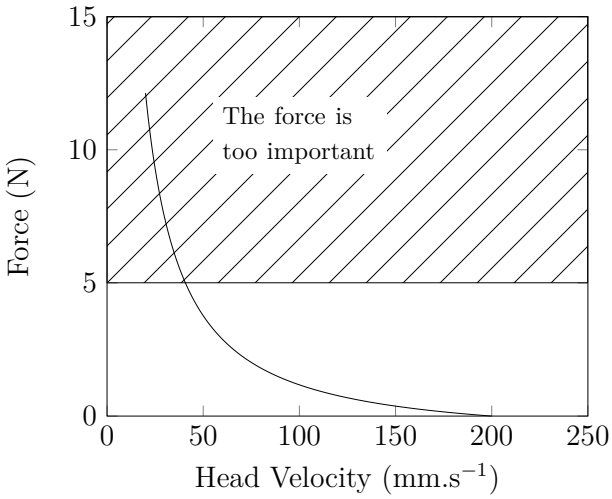

Figure 16: Separating force as a function of the printing head velocity.

- Lower limit: if the pressure is too low (for example less than 1 MPa), the filling of the porosities between the successive deposited layers could be less efficient. This value obviously depends on the rheology of the deposited layer.

Figure 16 shows the separating force exerted on the printing head as a function of the head velocity. Depending on the design of the printing machine, a too high of a force (for example higher than 5 Newton) may prevent respecting the prescribed gap between head and substrate.

These different requirements reduce the possible printing velocities between 40 mm/s and 140 mm/s.

The thickness of the deposited layer will lie between 0.06 mm and 0.08 mm and its width between 0.5 mm and 1.3 mm.

3.2. Influence of the gap between the printing head and the substrate

The gap e between the head and the substrate is varied between 0.1 mm and 0.4 mm. For a gap greater than the nozzle diameter, 0.4 mm, there is a free surface flow between the nozzle exit and the substrate and the polymer deposition mechanism will change (surface tension spreading instead of shear and pressure spreading).

Figure 17 shows the dimensions (thickness and width) of the deposited layer as a function of the head velocity for the different gaps. Referring to Eq. (16), the printing head velocity range will vary with the prescribed gap. In each case the deposited thickness varies between half the gap value and the gap value. The width varies between the internal and external dimensions of the printing head. For a given printing head velocity, the deposited thickness increases with the gap and its width decreases.

Figure 18 shows the pressure and the separating force as a function of the head velocity for the different gaps. The upper limiting value for the pressure and separating force is only reached for the smallest gap (0.1 mm) and head velocity V lower than 40 mm/s. For $e = 0.4$ mm and $e = 0.3$ mm, the spreading pressure is always below the lower limiting value. The pressure is above this value, with a gap of 0.2 mm, for $V < 30$ mm/s, and with a gap of 0.1 mm for $V < 150$ mm/s.

3.3. Influence of the extrusion flow rate Q

Figure 19 shows the dimensions of the deposited layer as a function of the printing head velocity for polymer rates ranging between 12 and 40 mm^3/s and a gap between head and substrate equal to 0.2 mm. The interval of variation of the velocity of the printing head has been set according to Eq. (16) and limited to a maximum velocity of 600 mm/s. Both thickness and width increase when the polymer flow rate increases.

Figure 20 shows the pressure P_0 at the nozzle and the separating force as a function of the printing head velocity for four polymer flow rates. The printing head velocity must be below a certain value to satisfy the low spreading pressure criteria: $V = 150$ mm/s for $Q = 12$ mm^3/s; $V = 280$ mm/s for $Q = 20$ mm^3/s; $V = 450$ mm/s for $Q = 28$ mm^3/s. Concerning the limitation of the separating force to 5 Newton, it does not impose additional requirements on the printing head velocity.

4. Conclusions

The spreading of the molten polymer in the extrusion additive manufacturing process has been investigated using numerical finite element computations as well as analytical calculations. The development of the free surface, the shape of the deposited layer and the pressure distribution have been computed in the Newtonian isothermal case. Two different ratios between the polymer flow rate and the printing head velocity have been considered. In both situations the spreading distance of the polymer in front of the printing head is of the same order of magnitude as the spreading distance in the lateral directions. The polymer rate is quite homogeneous in the spreading deposit width. This opens the route for a simplified analytical model which allows predicting the influence of processing and geometrical parameters. Characteristic results are, for example, the deposited thickness which decreases when the printing head velocity increases and lies between half the gap value (between the printing head and the substrate) and the gap value. Another example is the pressure at the nozzle, which decreases when the head velocity is increased. This model also provides relationships between the geometry of the head and the processing parameters to obtain a continuous deposited layer without polymer build up in front of the head. Introducing additional conditions on the pressure at the nozzle and on the separating force between the printing head and the substrate allows defining an effective printing domain.

Both numerical and analytical models are based on several approximations which need to be discussed.

- As pointed out by our preliminary heat transfer approach, the polymer spreading is only isother-

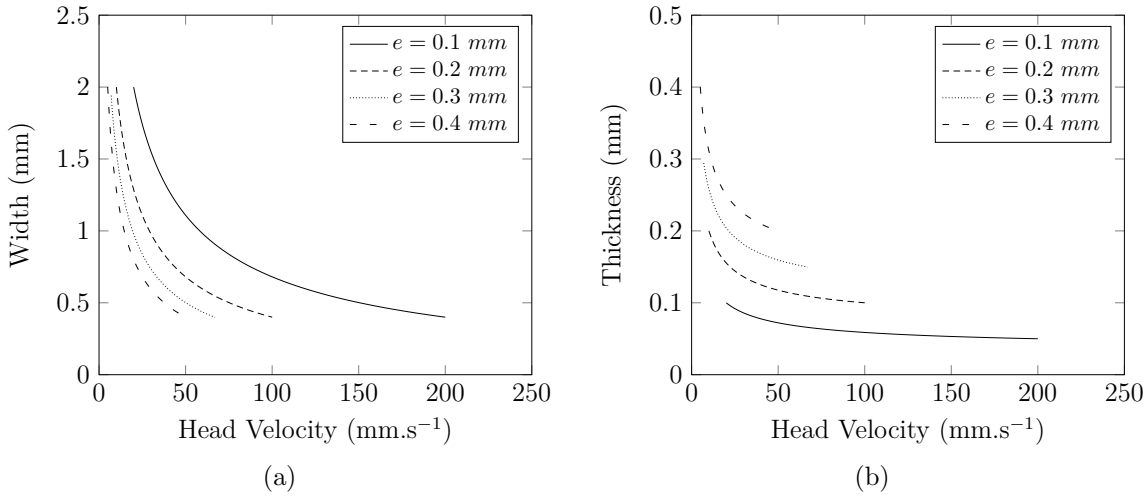

Figure 17: Width (a) and thickness (b) and of the deposited layer for four gap values.

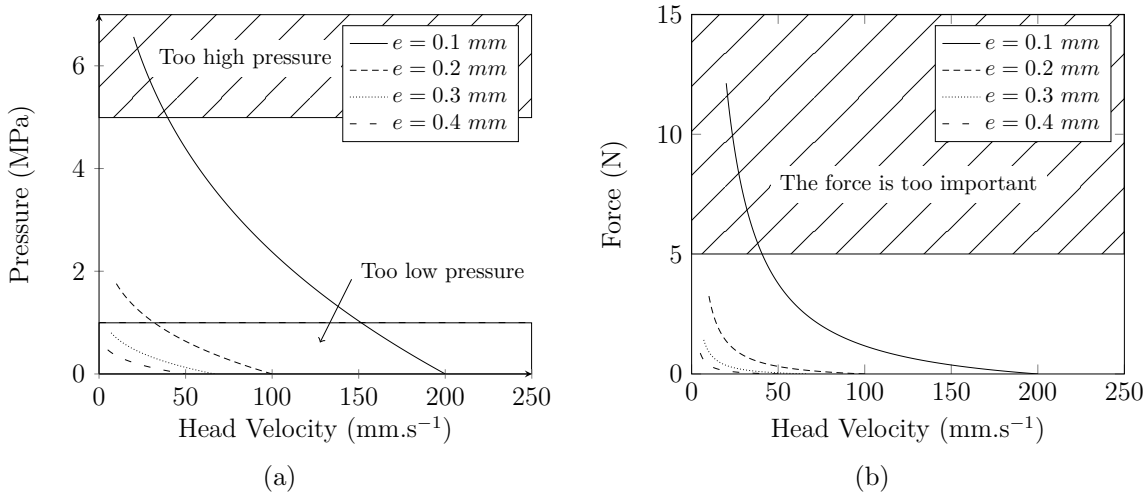

Figure 18: Pressure (a) and separating force (b) as a function of the head velocity for four gap values between head and substrate.

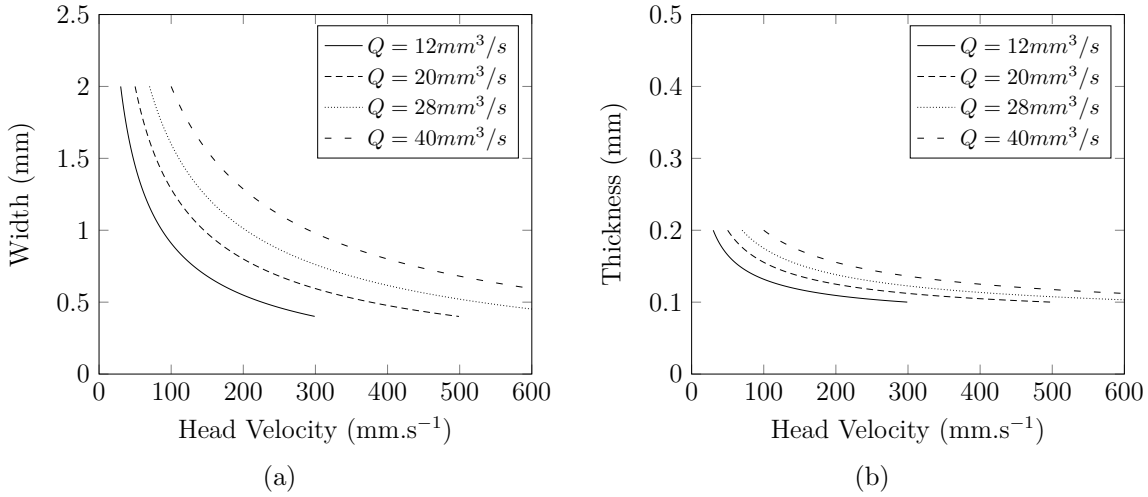

Figure 19: Width (a) and thickness (b) of the deposited layer as a function of the printing head velocity for four polymer flow rates: 12, 20, 28, and 40 mm^3/s.

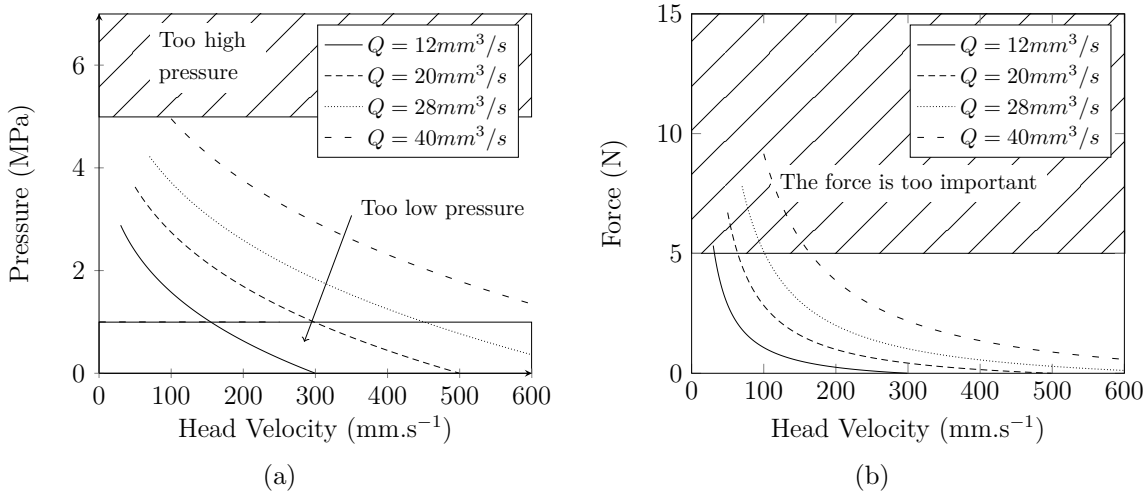

Figure 20: Pressure (a) and separating force (b) of the deposited layer as a function of the printing head velocity for four polymer flow rates: 12, 20, 28, 40 mm^3/s.

mal for important printing head velocities and printing gaps values. Moreover, the initial temperature profile at nozzle exit may be heterogeneous depending on the heating process in the printing head. This nozzle temperature distribution can significantly affect the spreading process.

- The non-Newtonian behavior of the polymer has been accounted for in the analytical model as an equivalent viscosity at an average shear rate between the printing head and the substrate. In fact, the flow kinematics is much more complex than a pure shearing flow at a constant shear rate.

- The substrate is only planar for the first deposited layer. For the next ones, the substrate may be wavy.

All these geometrical, non-isothermal, non-Newtonian complexities need to be accounted for in an advanced numerical model.

References

[1] B. D. Vogt. Morand lambla plenary lecture. In *33rd Annual Meeting of the Polymer Processing Society*, Cancun (Mexico), 2017.

[2] M. Nikzad, M. S. Hasan, I. Sbarski, and A. Groth. A study of melt flow analysis of an abs-iron composite in fused deposition modelling process. *Tsinghua Sci. Technol.*, 14(S1):29–37, 2009.

[3] M. E. Mackay, Z. R. Swain, C. R. Banbury, D. D. Phan, and D. A. Edwards. The performance of the hot end in a plasticating 3D printer. *J. Rheol.*, 61(2):229–236, 2017.

[4] D. D. Phan, Z. R. Swain, and M. E. Mackay. Rheological and heat transfer effects in fused filament fabrication. *J. Rheol.*, 62(5):1097–1107, 2018.

[5] A. Bellini. *Fused deposition of ceramics: A comprehensive experimental, analytical and computational study of material behavior, fabrication process and equipment design.* PhD thesis, Drexel University, 2002.

[6] C. Bellehumeur, L. Li, Q. Sun, and P. Gu. Modeling of bond formation between polymer filaments in the fused deposition modeling process. *J. Manuf. Processes*, 6(2):170–178, Jan 2004.

[7] Q. Sun, G. M. Rizvi, C. T. Bellehumeur, and P. Gu. Effect of processing conditions on the bonding quality of FDM polymer filaments. *Rapid Prototyping J.*, 14(2):72–80, 2008.

[8] R. S. Crokett. *The liquid to solid transition in stereodeposition techniques.* PhD thesis, University of Arizona, 1997.

[9] B. N. Turner, R. Strong, and S. A. Gold. A review of melt extrusion additive manufacturing processes: I. process design and modeling. *Rapid Prototyping J.*, 20(3):192–204, 2014.

[10] J. Du, Z. Wei, X. Wang, J. Wang, and Z. Chen. An improved fused deposition modeling process for forming large-size thin-walled parts. *J. Mater. Process. Technol.*, 234:332 – 341, 2016.

[11] R. Comminal, M. P. Serdeczny, D. B. Pedersen, and J. Spangenberg. Numerical modeling of the strand deposition flow in extrusion-based additive manufacturing. *Addit. Manuf.*, 20:68 – 76, 2018.

[12] H. Xia, J. Lu, and G. Tryggvason. Fully resolved numerical simulations of fused deposition modeling. part ii – solidification, residual stresses and modeling of the nozzle. *Rapid Prototyping J.*, 24(6):973–987, 2018.

[13] M. Khalloufi, Y. Mesri, R. Valette, E. Massoni, and E. Hachem. High fidelity anisotropic adaptive variational multiscale method for multiphase flows with surface tension. *Comput. Methods Appl. Mech. Eng.*, 307:44–67, 2016.

[14] R. Valette, T. Coupez, C. David, and B. Vergnes. A direct 3d numerical simulation code for extrusion and mixing processes. *Int. Polym. Proc.*, 24(2):141–147, 2009.

[15] S. Osher and J. A. Sethian. Fronts propagating with curvature-dependent speed: Algorithms based on Hamilton-Jacobi formulations. *J. Comput. Phys.*, 79(1):12–49, 1988.

[16] T. J. Coogan and D. O. Kazmer. In-line rheological monitoring of fused deposition modeling. *J. Rheol.*, 63(1):141–155, 2019.

[17] J.-F. Agassant, P. Avenas, P. J. Carreau, B. Vergnes, and M. Vincent. *Polymer processing: principles and modeling.* Carl Hanser Verlag GmbH Co, 2017.